Revista Brasileira de Física, Vol. 6, Nº 2, 1976

Elastic Scattering of 3 ~ and a Particles on Sb, Sn and Te*

A. T. M. MENDES**, N. UETA and M. N. RAO
Laboratdrio Pelletron – Instituto de Física da USP, São Paulo S

Recebido em 23 de Janeiro de 1976

The angular distributions of elastic scattering of 3 He and a particles of about 20 MeV from nuclei of Z approximately 50 were measured. Optical model parameters which reproduce the experimental data have been systematically determined.

Foram medidas as distribuições angulares do espalhamento elástico de ^{3}He rtículas a de cerca de 20 Mev por núcleos com Z da ordem de 5.0. Foram determinados sistematicamente os paramêtros do Modelo Optico que reproduzem os dados experirnentais.

1. INTRODUCTION

As part of a systematic study of ^{3}He and a particle induced reactions in the region of Tin, Antimony and Tellurium nuclei, the angular distributions of elastically scattered ^{3}He and a particles from these nuclei, were measured at the available incident energy of about 20 MeV. A compilation of ^{3}He and a particle optical model parameters fornuclei throughout the periodic table has been published by Perey and Perey[1]. More recent data and analysis for $Z \approx 50$ are available in Refs. (2) and (3). Nevertheless, at the incident energies available from the Pelletron accelerator, the data are scarce in the region of nuclei studied.

---

* Work submitted in partial fulfillment of the requirements for the degree of Master of Science (A.T.M.M.).

** Fellow of the FAPESP (Process 71/1435).

2. EXPERIMENTAL TECHNIQUES AND RESULTS

2.1.- TARGETS AND APPARATUS

The targets of about 100 - 150 $\mu g/cm^2$ were prepared by vacuum evaporation of enriched material onto 20 $\mu g/cm^2$ carbon foils. The target materiais were obtained from the Stable Isotopes Division, Oak Ridge National Laboratory, Oak Ridge, Tennessee, USA. The enrichment factors of the samples used to prepare the targets for the present experiments are given in Table 1. The absolute cross sections were determined assuming that, at the incident energies utilized (~20 MeV), the cross section at the forward angles ($\leq 45^0$) is only due to Rutherford scattering. The errors in the absolute cross sections are estimated to be 10%. A 5% error due to nonuniformity of the targets is included.

The beams of ^3He and a particles, produced in an externa1 source of the charge exchange type[4], were injected through a single focussing 90^0 magnet (ME-20) into the Pelletron 8UD tandem accelerator of the University of São Paulo[5].

After acceleration, the beam is energy analysed in a double focussing 90^0 magnet (ME-200). The magnet calibration constant was obtained by measurements of (p,n) and (α,n) thresholds[6,7] and the study od the resonance at 14231 keV in the $^{12}C(p,p)$ reaction .

With the aid of a switching magnet and a quadrupole doublet, the energy analysed beam is transported to the entrance collimator of a large (ϕ = 1m) scattering chamber.

The scattering chamber (Fig.1) was forrnely usedat the University of Wisconsin to study the H(p,p)H reaction[9]. After modifications for use with solid targets, this chamber was installed and the centering tested to a precision better than 1%.

A beam spot diameter of 4 mm could be obtained with the aid of the 105 cm long entrance collimator with defining slits of 3.5 mm diameter.

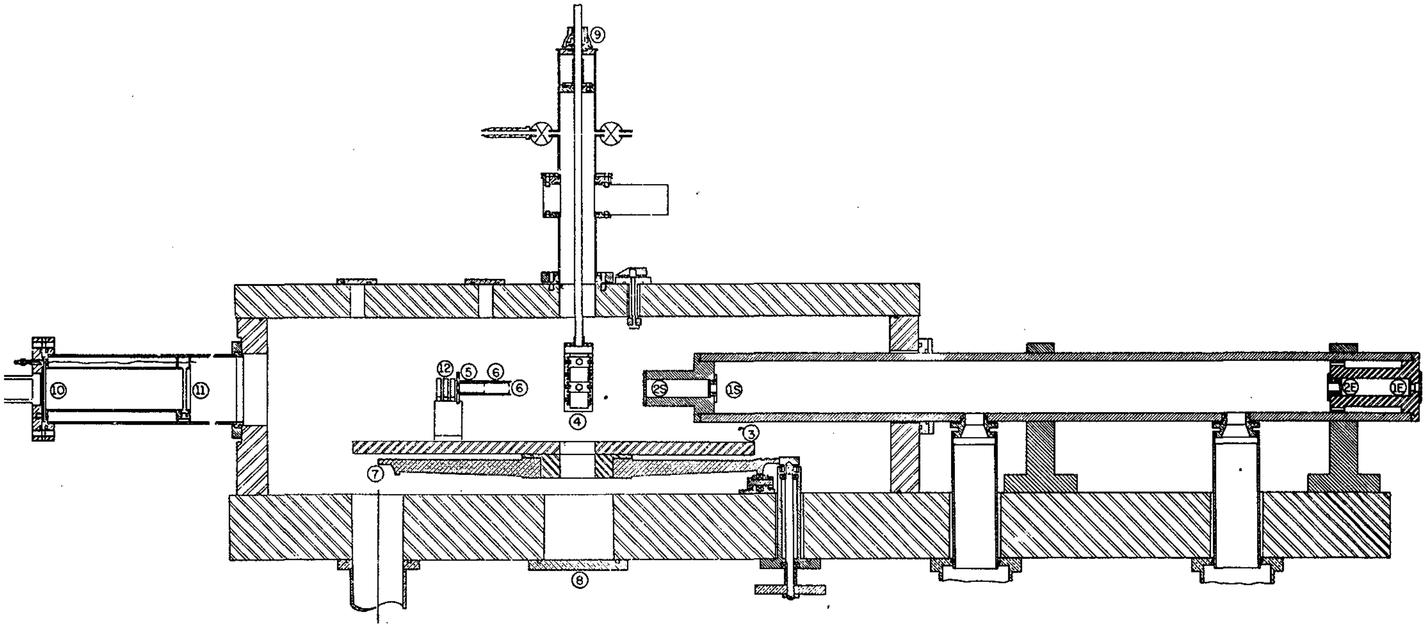

Fig.1 - Vertical cross sectional view of the chamber. 1S and 1E defining slits of the beam entrance collimator; 2S and 2E antiscattering slits; 3. movable arm; 4. target holder; 5. defining slits of the detector collimator; 6. antiscattering slits of the detector collimator; 7. angle wheel; 8. connectors for detector signal output; 9. system for target positioning; 10. Faraday cup; 11. electric supressor of Faraday cup; 12. detector.

The modified chamber allows for the changing of up to 4 targets without breaking the vacuum. Up to five silicon surface barrier detectors could be mounted on a movable arm and the positioning of the detectors could be read to a precision of 1'. The detector, provided with collimating and antiscattering slits, subtended a solid angle of -4 × 10^{-4} steradian and had an angular resolution of ±1.4°.

The beam current collected in a Faraday cup, which had geometrical and electrical suppression, was integrated to within a precision of 2%. A monitor detector, positioned at 45° to the beam, provided a constant check on the measurements.

Data were accumulated in a Honeywell DDP 516 Computer used in the multichannel mode and later transfered to a magnetic tape through an IBM / /360-44 Computer[10].

2.2.- THE ELASTIC SCATTERING ANGULAR DISTRIBUTIONS

The angular distributions were measured from 10° to 145° in 5° steps for the following cases:

$^{124}Sn\ (^3He,\ ^3He)^{124}Sn$,	22.35 MeV,
$^{123}Sb\ (\alpha,\ \alpha)^{123}Sb$,	19.95 MeV,
$^{124}Te\ (\alpha,\ \alpha)^{124}Te$,	19.3 MeV,
$^{124}Sn\ (\alpha,\ \alpha)^{124}Sn$,	19.5 MeV,
$^{123}Sb\ (^3He,\ ^3He)^{123}Sb$,	19.5 MeV,
$^{124}Te\ (^3He,\ ^3He)^{124}Te$,	19.52 MeV,
$^{122}Te\ (^3He,\ ^3He)^{122}Te$,	19.52 MeV.

The statistical uncertainties varied from less than 1% in the forward angles to about 3% in the backward angles. In the case of $^{124}Sn + {^3He}$ angular distribution, some of the backward angle data could not be obtained with statistical accuracy better than 14%.

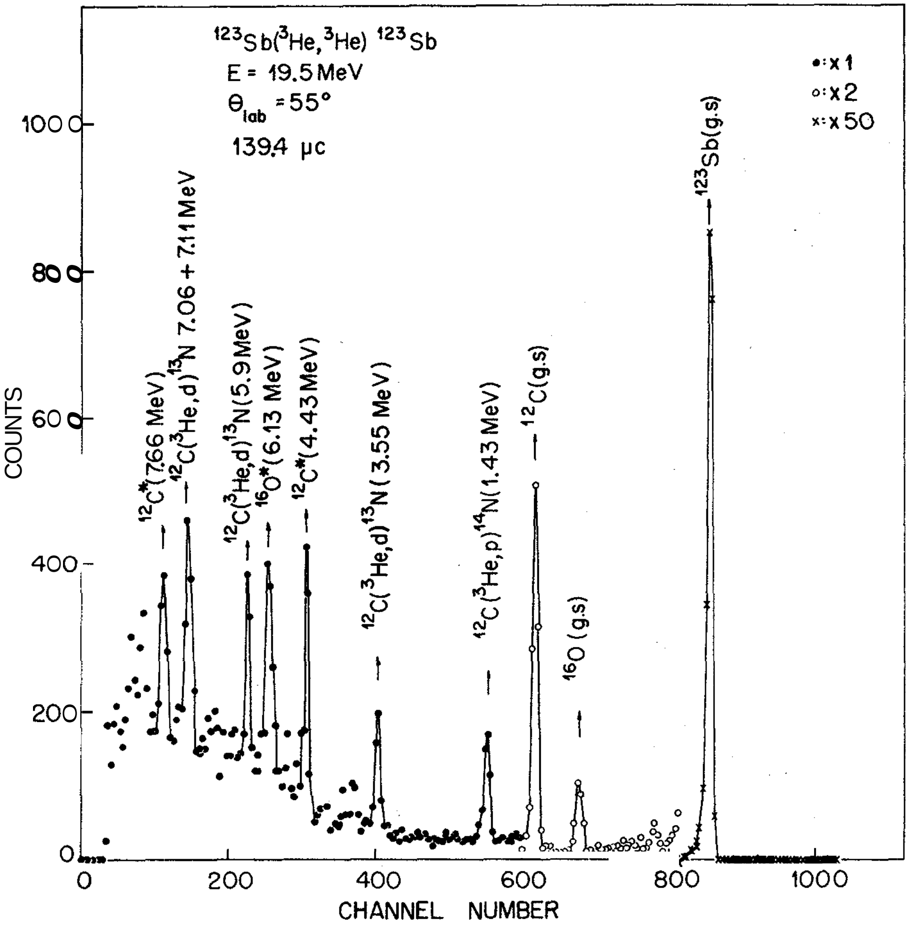

Fig.2 - Typical spectrum of elastic scattering of ^{123}Sb(^{3}He,^{3}He)^{123}Sb.

The energy resolution varied from 30 to 70 keV due to the energy loss of the beam in the target, kinematical broadening and detector resolution. An improvement of the energy resolution was obtained when a positive bias of 5 kV was applied to the target holder.

Particle identification was not considered necessary as the other reactions were of negligible cross section or were kinematically well separated from the elastic events.

Typical spectra for ^{3}He on ^{123}Sb and a on ^{124}Te are shown in Figs.2 and

On account of the rather low incident energy, the angular distributions do'not show any diffraction structure, but are rather srnooth. The data reduced to the center of rnass systern are shown in Table 2.

3. OPTICAL MODEL ANALYSIS

3.1. - FORM OF THE OPTICAL POTENTIAL

The analyses of the experimental elastic angular distributioris were performed with the aid of an optical model search code MODOPT[11] which could be run on both the IBM/360-44 and the B-6700 computers. The poreniial used was of the forrn:

$$U(r) = V_c(r) - \{V_0 f(r,r_0,a_0) + i\left[W_v f(r,r_v,a_v) + W_s g(r,r_s,a_s)\right]\} +$$

$$+ \left(\frac{\hbar}{m_\pi c}\right)^2 \{V_{so}\frac{1}{r}\frac{d}{dr} f(v,r^R_{so},a^R_{so}) + i\, W_{so}\frac{1}{r}\frac{d}{dr} f(r,r^I_{so},a^I_{so})\}\vec{\sigma}\cdot\vec{\ell}$$

with

$$f(r,r_x,a_x) = \left[1 + \exp\frac{r-r_x A^{1/3}}{a_x}\right]^{-1} \quad \text{(Woods-Saxon)},$$

$$g(r,r_x,a_x) = \exp\left[-\{(\frac{r-r_x A^{1/3}}{a_x})\}^2\right] \quad \text{(Gaussian)},$$

$$g(r,r_x,a_x) = 4\, a_x \frac{d}{dr} f(r,r_x,a_x) \quad \text{(Woods-Saxon derivative)}$$

and

$$V_c(r) = \begin{cases} \dfrac{Z_I Z_T e^2}{2R_c}\left(3 - \dfrac{r^2}{R_c^2}\right), & \text{for } r < R_c\,, \\[2ex] \dfrac{Z_I Z_T e^2}{r} & \text{for } r > R_c\,, \end{cases}$$

where Z_I and Z_T are the atomic number of the incident particleandtar- get respectively and

$$R_c = r_c \; A^{1/3} \; .$$

17 partial waves were necessary in the calculations. The Coulornb radius, r_c, was fixed at 1.25F as suggested by Luetzelschwab *et al.*[12].

3.2. - FOUR PARAMETER GRID SEARCH

In general, the optical potentials are determined with ambiguities. Both discrete and continuous arnbiguities of the real potentiai are discussed by several authors[13-16].

There exist discrete values of the real well depth for a fixed radius which give almost the same fit (discrete ambiguity). The real potentials determined in the discrete ambiguity have the same depth at the radius of strongest absorption R_A which is related to the preferencial partial wave by the relation:

$$R_A = \frac{\eta + \{\eta^2 + \ell\,(\ell+1)\}^{1/2}}{k} \; ,$$

where η is the Coulomb constant, k, the wave number and ℓ is chosen so that $Re(S_\ell) = 0.5$ (Ref.17), S being the scattering rnatrix.

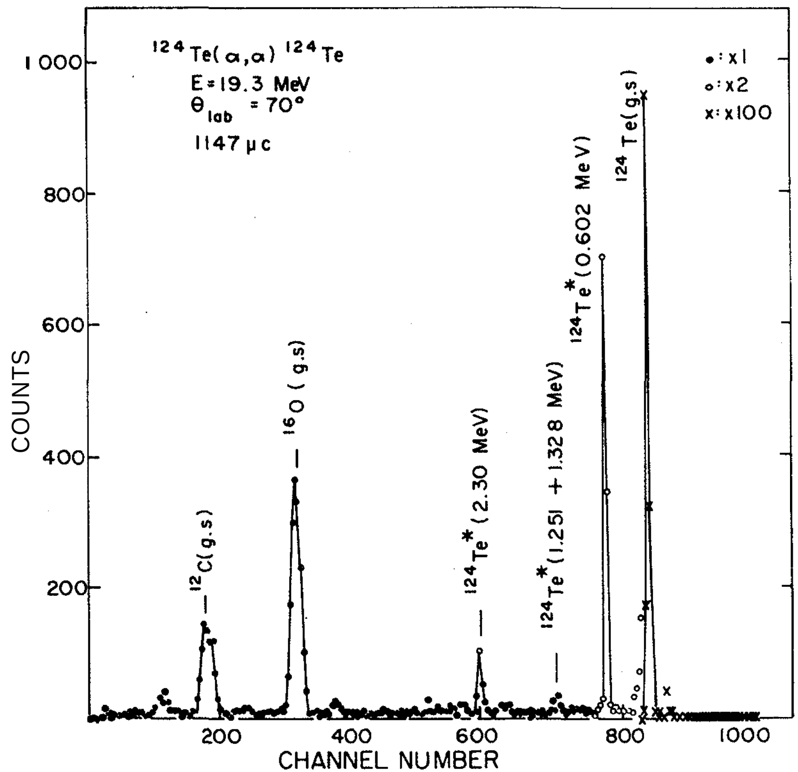

Fig.3 - Typical spectrum of elastic scattering of $^{124}Te(\alpha,\alpha)^{124}Te$.

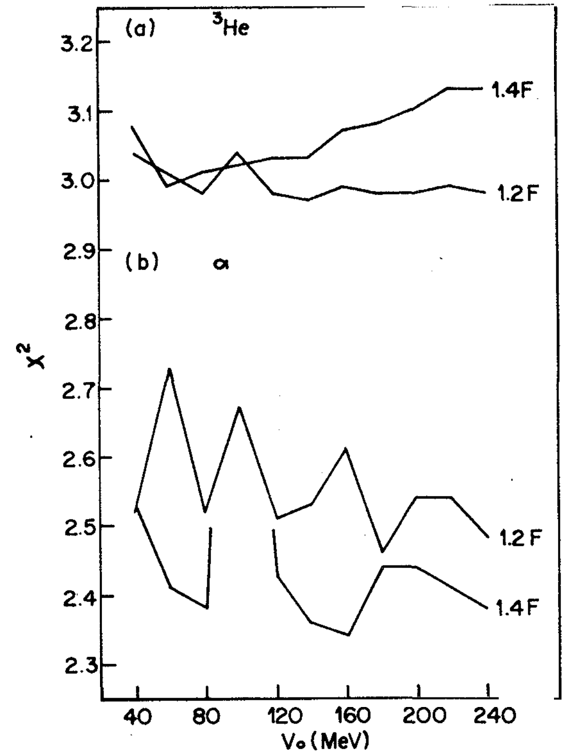

Fig.4 - χ^2 plot obtained in the grid search as a function of V_0 for a) ^3He on ^{123}Sb, b) α on ^{123}Sb.

Although the depths are completely different, for $r > R_A$ all potentials have the same trend and similar fits to the elastic scattering data are obtained[14,18,19]. The discrete ambiguity corresponds to the inclusion of an additional half wave length of the wave function of the most significant partial wave into the potential well[15].

The continuous ambiguity occurs for values of r_0 and V_0 such that the product $V_0\, r_0^n$ is constant.

Two new parameters were introduced by Greenlees et al.[20] to characterize the different potential families: J_0, thevolume integral per pairof particles, $<r_0^2>^{1/2}$, the root mean square radius.

For the Woods-Saxon form factor,

$$J = \frac{4\pi}{3} V_0 R_0^3 \left[1 + \left(\frac{\pi a_0}{R_0}\right)^2 \right]$$

with $R_0 = r_0 \; A^{1/3}$ and $J_0 = J/(A_I A_T)$, A_I and A_T are the mass numbers of the incident particle and of the target respectively. J_0 varies in discrete steps of 100 MeV.F^3 for the different families[19].

The root mean square radius for the Woods-Saxon form factor is given by,

$$<r_0^2>^{1/2} = \left[\frac{3}{5} R_0^2 \, \{1 + \frac{7}{5} \, (\pi a_0/R_0)^2\} \right]^{1/2}$$

and should be constant as a function of V, within one family.

Based on a procedure suggested by Baugh[15], a grid search on the parameters V, and r, was performed with the ^{123}Sb + α data. Volume absorption was used in this procedure. No spin-orbit term was included. V, was varied from 40 to 240 MeV in steps of 20 Mev and r_0 from 1.15 to 1.4 F in steps of 0.05 F. For each (V_0, r_0) selected pair, a simultaneous search was performed on the four parameters a_0, W_v, r_v and a_v.

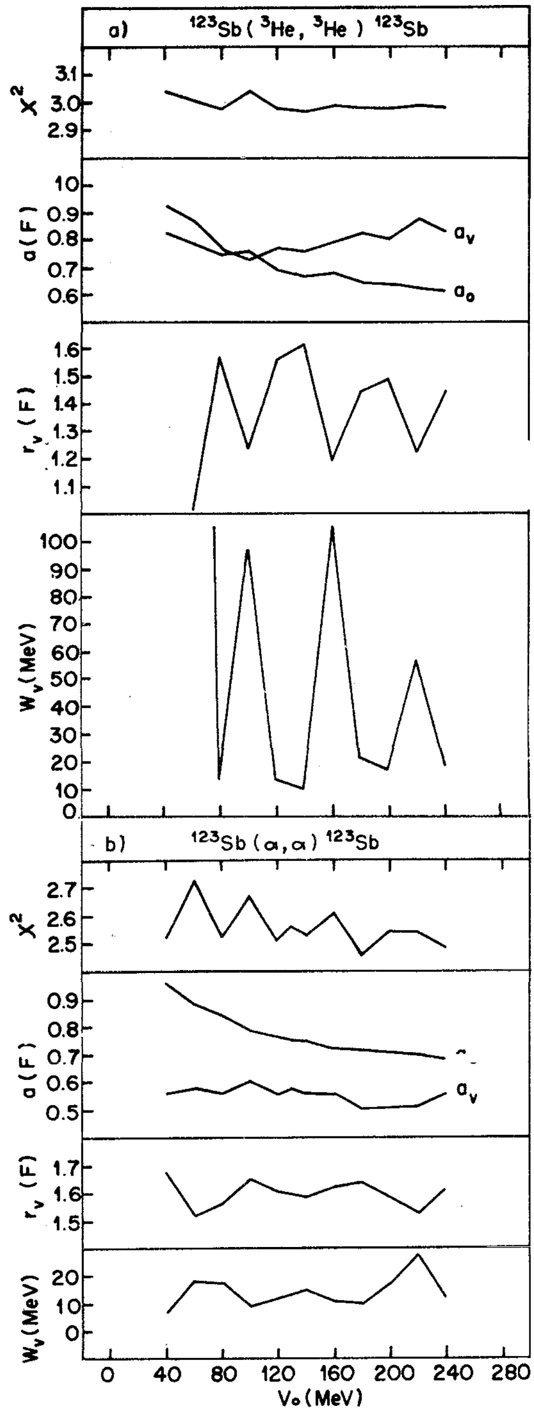

Fig.5- Variation of the optical model parameters as a function of V_0 a) for ^{123}Sb + ^{3}He, b) for ^{123}SB + α.

The minimum χ^2 values were obtained with r_0 = 1.4 F for values of V_0 at intervals of -80 MeV. For r_0 = 1.2 F, even though the χ^2 minima were slightly worse, a spacing of -40 MeV between the minima was found. No visual distinction could be made between the fits obtained with r_0=1.2 F and r_0 = 1.4 F.

A four parameters grid search was also performed with the ^{123}Sb + ^{3}He data, for r_0 = 1.2 F and 1.4 F. For r_0 = 1.2 F, a V_0 spacing of -40 MeV between the χ^2 minima was obtained. However, for r_0 = 1.4 F, only one minimum with V_0 = 40 MeV was found.

These results are surnmarized in Fig.4, while the variation of the individual parameters as a function of the real depth V_0 for r_0 = 1.2 F, is presented in Fig.5. Starting from the parameters which gave minima for r_0 = 1.2 F and 1.4 F in $^{123}Sb(\alpha,\alpha)^{123}Sb$ analysis, and for r_0= 1.2 F in $^{123}Sb(^{3}He,^{3}He)$ Sb analysis, a five parameter search was performed. The resulting parameters, together with the J_0 and $<r_0^2>^{1/2}$ values are shown in Tables 3 and 4, for a particles and ^3He respectively. The parameters marked with (*) in Table 3 and Table 4 were used as starting parameters for the other angular distributions. It is known that the best fits are obtained when the potential depth is 120-180 MeV for ^3He and 160-240 MeV for α particles. With this criterion, the parameters given in Table 5 were chosen as the most adequate and the corresponding fits are shown in Fig.6.

3.3.- THE IMAGINARY PART OF THE OPTICAL POTENTIAL

Maintaining the parameters of the real potentials listed in Table 5, attempts were made to determine the surface absorption potentials (Woods--Saxon derivative form factor) for the Sn and Te angular distributions. In the case of Sb, a more detailed study was performed. The results are included in Table 3 and Table 4. No essential differences in the quality of the fits were observed between volume and surface absorption potentials, as expected, since the angular distributions are rather smooth[14,18,19]

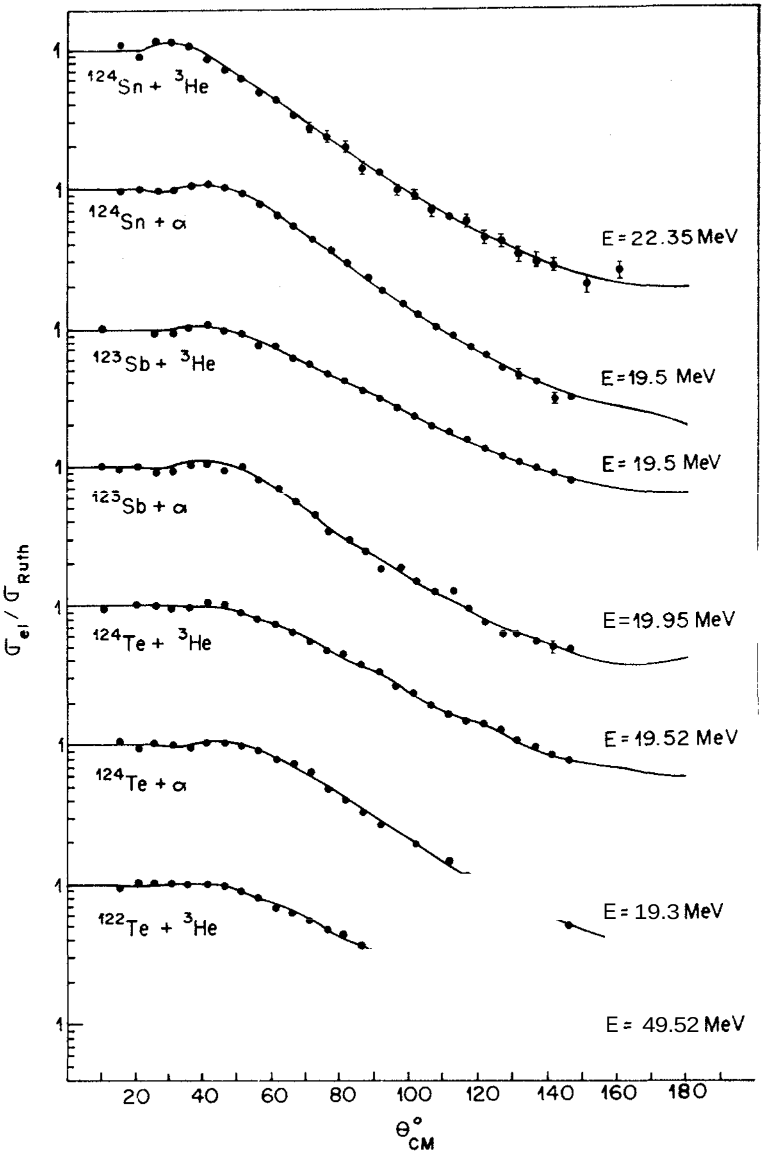

Fig. 6 - Ratio of the experimental cross section to Rutherford cross section for elastic scattering of ^{3}He and a particles. The curves are calculated with the best **fit** parameters of Table 5. The error bars are shown when larger than the size of the point.

In the case of angular distributions with a marked diffraction pattern, a surface imaginary term gives, in general, a better fit than a volume term[21].

3.4. - THE SPIN-ORBIT TERM

A spin orbit term of -2 MeV, as suggested by Luetzelschwab *et al.*[12], Urone *et al.*[14] and by Cage *et al.*[19], was included in the analysis without any significant improvement in the fit, as was expected for a structureless angular distribution. As no polarization data pertinent to the present results. were available, the spin-orbit term was not included in the final fit.

4. DISCUSSION AND CONCLUSIONS

An examination of Table 4 shows that the variation of the parameters follows the systernatic behavior observed by Cage et *al.*[19] and by Baugh[15], namely: a, and r_V decrease whereas w_s or w_V and a_v increase for increasing V_0.

The radius of strongest absorption of the potentials (Table 4) which fit the ^{3}He scattering on Sb is 9.9 F and corresponds to R = 7, whereas for α scattering on Sb (Table 3), R_A = 10.3 F which corresponds to R = 9 (Fig.7). These values are in agreement with Cage *et al.*[16] and Weisser *et al.*[18] although the corresponding R values differ slightly from those calculated imposing the condition that $Re(S_R) = 0.5$ (Ref.17).

The values of V_0 obtained in the grid search of $^{123}Sb(\alpha,\alpha)^{123}Sb$ are plotted as a function of *r,* in Fig.8. The mean value of J_0 varies by about 100 MeV F for adjacent families

For some families, the valueç of $<r_0^2>^{1/2}$ were calculated for different values of *r*,. These results are shown in Fig.9. A slight variation of the root mean square radius, as a function of *r*,, is observed in agreement with Cage et *al.*[19], although it had been introduced as a constant within one family.

No preference for a surface or volume imaginary form factor was detected.

As a spin-orbit term was not necessary, effects due to the target spins were not looked for.

As can be seen in Fig. 6, all the a particle angular distributions (19.3 - 19.9 MeV) have the same overall trend. A similar behaviour is also observed for ^{3}He, except in the case of ^{124}Sn measured at a slightly higher energy (22.3 MeV). The comparison between a particle and ^{3}He angular distributions measured at the same energy shows a larger diffuseness for a particle than for ^{3}He. Bock et *al.*[22] have observed a larger diffuseness for ^{3}He than for a particle with data obtained at equal momenta.

Systematic measurements at higher energies are needed to observe the dependence of optical model potential on more complicated effects such as mass number of targets, spin-spin interactions and isotopic spin.

We would like to thank Prof. O. Sala for his constant interest in this work. The assistance of Dr.T. Polga and Mr. A. Szanto de Toledo in the operation of the rnachine is gratefully acknowledged. We also express our thanks to Mr. M. Cappello and the staff of the work-shop fur their help during the modification and installation of the scattering chamber; to Mr. M. Ferrareto, Mr. A. Telles and the computer staff for assistance in the acquisition of data. We are greatly indebted to the University of Wisconsin for providing us the scattering chamber.

Target	Chemical Composition	%
^{122}Te	metallic	96.21
^{124}Te	metallic	96.21
^{124}Sn	SnO_2	94.74
^{123}Sb	SbO_2	99.05

Table 1 - Enrichment factors of the targets studied.

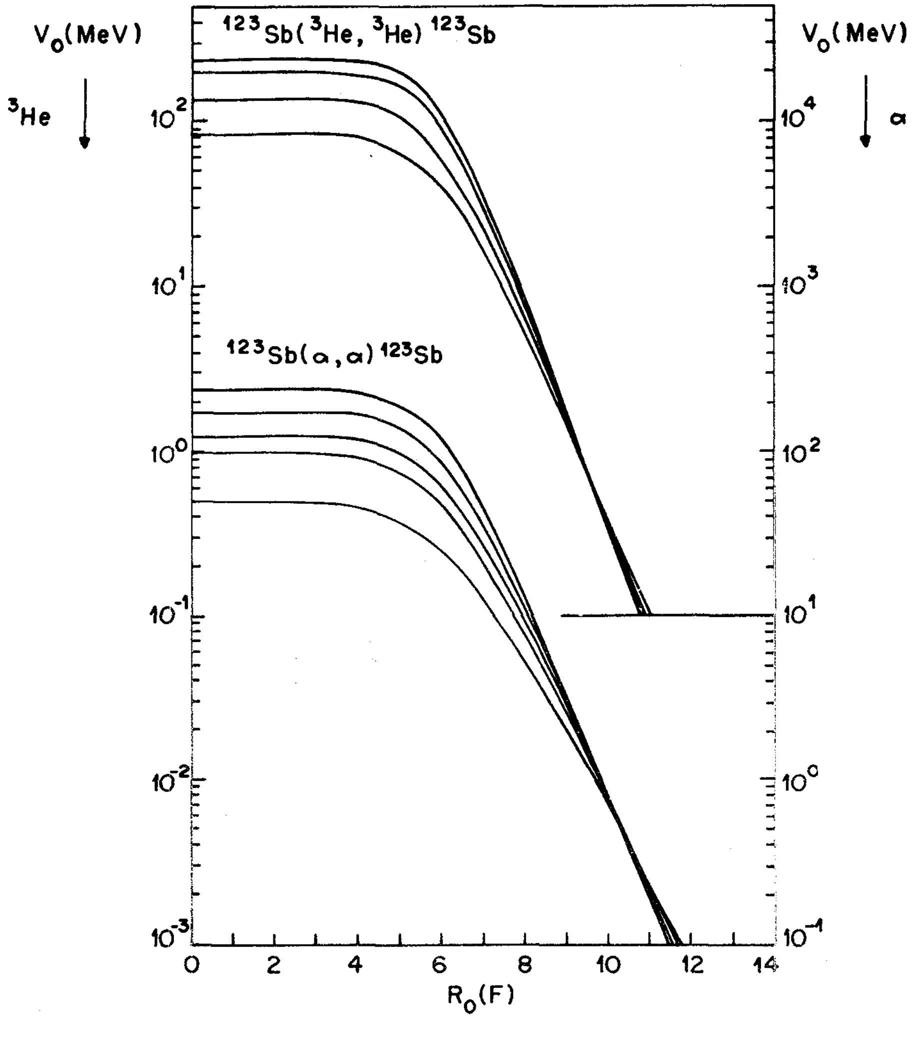

Fig.7 - Plots of the depth of real optical potentials of Tables 3 and 4 as a function of the real radius R .

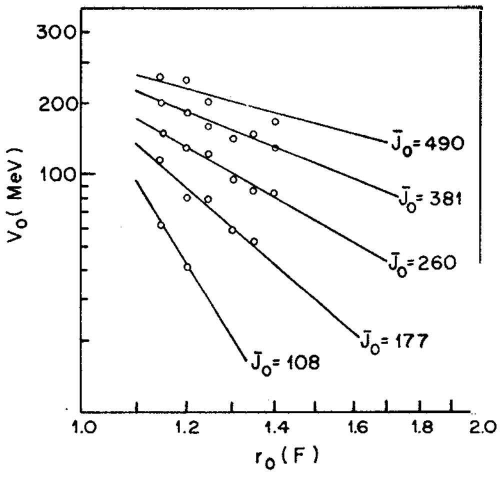

Fig.8 - Variation of potential V as a function of r_0 obtained in the search for $^{123}Sb(\alpha,\alpha)^{123}Sb$. The corresponding $\bar{J}_0$ values of each family are also shown.

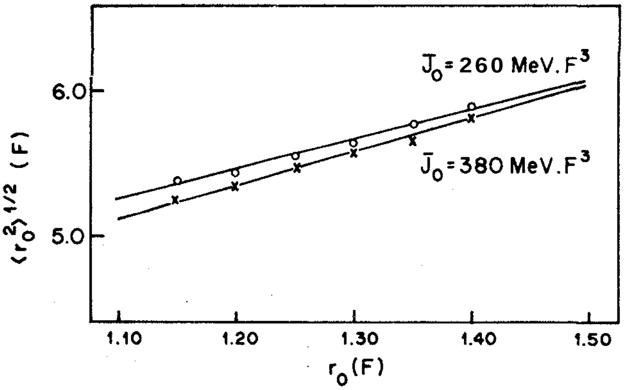

Fig.9 - Variation of $\langle r_0^2\rangle^{1/2}$ as a function of **r** . The open circles correspond to the family with $\bar{J}_0$ = 260 MeV.F^3 and the crosses to $\bar{J}_0$ = 380 MeV.F^3.

$^{124}Sn(^{3}He, ^{3}He)^{124}Sn$ E = 22.35 MeV		
θ^{o}_{cm}	$\sigma_{el}/\sigma_{Ruth.}$	$\epsilon_{abs.} \times 10^{2}$
15.36	1.097	7.3
20.48	0.909	6.0
25.59	1.148	7.6
30.70	1.129	7.5
35.80	1.075	7.1
40.90	.866	5.7
45.99	.724	4.8
51.07	.619	4.2
56.24	.486	2.9
61.21	.441	3.0
66.26	.344	2.4
71.31	.274	1.9
76.34	.243	1.8
81.37	.205	1.4
86.39	.142	1.0
91.39	.136	.93
96.39	.10	.72
101.37	.092	.69
106.35	.0653	.62
111.31	.064	.53
116.26	.060	.60
121.21	.047	.42
126.14	.042	.41
131.07	.034	.36
135.99	.0[illegible]	.39
140.90	.029	.27
150.70	.021	.29
160.48	.027	.35

$^{124}Sn(\alpha, \alpha)^{124}Sn$ E = 19.5 MeV		
θ^{o}_{cm}	$\sigma_{el}/\sigma_{Ruth.}$	$\epsilon_{abs.} \times 10^{2}$
15.48	0.957	5.6
20.63	0.961	5.7
25.78	0.973	5.7
30.92	0.966	5.7
36.06	1.063	6.3
41.19	1.072	6.2
46.31	1.045	5.4
51.42	.923	4.6
56.51	.786	3.8
61.60	.650	3.2
66.68	.544	2.6
71.74	.441	2.1
76.79	.359	1.7
81.82	.286	1.4
86.84	.234	1.1
91.85	.191	.94
96.84	.154	.75
101.82	.128	.65
106.79	.106	.55
111.74	.0905	.41
116.68	.0750	.41
121.60	.0668	.33
126.51	.0539	.30
131.42	.0473	.27
136.31	.0419	.20
141.19	.0316	.20
146.06	.0323	.21

$^{123}Sb(^{3}He, ^{3}He)^{123}Sb$ E = 19.5 MeV		
θ^{o}_{cm}	$\sigma_{el}/\sigma_{Ruth.}$	$\epsilon_{abs.} \times 10^{2}$
10.24	1.012	5.9
25.59	0.950	5.5
30.70	0.940	5.4
35.80	1.033	6.0
40.90	1.083	6.3
45.99	.980	5.7
51.07	.947	5.5
56.14	.771	4.5
61.21	.753	4.4
66.27	.626	3.6
71.31	.558	3.2
76.35	.466	2.7
81.38	.416	2.4
86.39	.341	2.0
91.40	.312	1.8
96.39	.263	1.5
101.38	.231	1.4
106.35	.197	1.2
111.31	.176	1.1
116.27	.158	.96
121.21	.136	.83
126.14	.112	.75
131.07	.111	.67
135.99	.0985	.61
140.90	.0905	.56
145.80	.0810	.52

$^{123}Sb(\alpha, \alpha)^{123}Sb$ E = 19.95 MeV		
θ^{o}_{cm}	$\sigma_{el}/\sigma_{Ruth.}$	$\epsilon_{abs.} \times 10^{2}$
10.32	1.022	5.1
15.48	0.949	4.8
20.64	1.024	5.1
25.79	0.927	4.6
30.93	0.927	4.6
36.07	1.028	5.1
41.20	1.072	5.4
46.32	.996	5.0
51.43	.995	5.0
56.53	.811	4.0
61.61	.702	3.5
66.69	.560	2.8
71.75	.450	2.3
76.80	.347	1.9
81.84	.303	1.6
86.86	.243	1.4
91.86	.186	1.2
96.86	.192	1.0
101.84	.154	.80
106.80	.129	.70
111.75	.129	.10
116.69	.0977	.50
121.61	.0794	.40
126.53	.0627	.40
131.43	.0640	.40
136.32	.0559	.30
[illegible]	[illegible]	[illegible]
146.07	.0501	.20

Table 2 - Ratio of the measured elastic cross section to the Rutherford cross section and the corresponding absolute error.

$^{124}Te(^3He,^3He)^{124}Te$ E = 19.52MeV		
θ^o_{cm}	$\sigma_{el}/\sigma_{Ruth.}$	$\epsilon_{abs.} \times 10^2$
15.36	0.961	4.6
20.47	1.028	4.9
25.59	1.018	4.8
30.69	0.953	4.6
35.80	0.991	4.7
40.89	1.070	5.1
45.98	1.049	5.0
51.06	.880	4.2
56.14	.815	3.9
61.20	.717	3.5
66.26	.640	3.1
71.30	.548	2.7
76.34	.476	2.3
81.37	.447	2.2
86.38	.382	1.8
91.39	.342	1.7
96.38	.264	1.4
101.37	.238	1.2
106.34	.198	1.0
111.30	.171	.87
116.26	.148	.78
121.20	.146	.77
126.14	.131	.72
131.06	.108	.55
135.98	.100	.50
140.89	.0872	.45
145.80	.0789	.45

$^{124}Te(\alpha,\alpha)^{124}Te$ E = 19.3 MeV		
θ^o_{cm}	$\sigma_{el}/\sigma_{Ruth.}$	$\epsilon_{abs.} \times 10^2$
15.48	1.037	5.0
20.63	0.954	4.6
25.78	1.055	5.1
30.92	1.037	5.0
36.06	0.955	4.6
41.19	1.030	4.9
46.31	1.047	5.1
51.42	1.000	4.8
56.51	.909	4.4
61.60	.814	3.9
66.68	.743	3.6
71.74	.639	3.1
76.79	.481	2.3
81.82	.405	1.9
86.84	.328	1.6
91.85	.274	1.3
101.82	.195	.73
111.74	.151	.73
116.28	.117	.56
121.60	.101	.50
126.60	.0912	.51
131.42	.0739	.36
136.31	.0624	.37
146.06	.0528	.33

$^{122}Te(^3He,^3He)^{122}Te$ E= 19.52 MeV		
θ^o_{cm}	$\sigma_{el}/\sigma_{Ruth.}$	$\epsilon_{abs.} \times 10^2$
15.36	0.961	4.1
20.48	1.031	4.4
25.60	1.027	4.4
30.70	1.021	4.4
35.81	1.003	4.3
40.91	1.004	4.3
46.00	.962	4.1
51.08	.896	3.8
56.15	.819	3.5
61.22	.792	3.4
66.28	.701	3.0
71.32	.550	2.4
76.36	.480	2.1
81.39	.442	1.9
86.40	.367	1.6
91.41	.305	1.3
96.40	.265	1.2
101.39	.229	1.0
106.36	.195	.88
111.32	.172	.77
116.28	.150	.67
121.22	.145	.65
126.15	.129	.58
131.08	.108	.54
136.00	.0922	.46
140.91	.0849	.42
145.81	.0819	.41

Table 2 - (Continued)

Energy (MeV)	Element	V_o (MeV)	a_o (F)	W_v (MeV)	r_v (F)	a_v (F)	W_s (MeV)	r_s (F)	a_s (F)	χ^2	J_o (MeV.F^3)	$\langle r_o^2\rangle^{1/2}$ (F)
r_0 = 1.2 F r_c = 1.25 F												
19.95	^{123}Sb	50.44*	0.936	3.72	1.827	0.388				1.41	113	5.784
		99.87*	0.822	12.01	1.640	0.538				1.28	214	5.540
		124.61*	0.733	7.46	1.708	0.498				1.32	264	5.461
		176.29*	0.737	9.39	1.676	0.506				1.31	373	5.372
		237.90*	0.701	11.68	1.645	0.501				1.30	489	5.305
		64.80	0.893				12.78	1.425	0.615	1.29		
		103.08	0.778				47.94	1.135	0.683	6.14		
		122.91	0.786				17.64	1.407	0.591	1.30		
		173.85	0.745				24.09	1.397	0.555	1.27		
		249.78	0.646				15.93	1.252	0.787	3.20		
19.5	^{124}Sn	42.07	0.952	3.87	1.831	0.532				0.22	95	5.816
		110.42	0.775	11.30	1.574	0.724				0.27	232	5.443
		124.42	0.796	9.29	1.630	0.517				0.63	264	5.484
		185.05	0.720	12.87	1.552	0.665				0.30	382	5.338
		239.22	0.684	12.45	1.534	0.719				0.57	487	5.272
		190.31	0.707				27.60	1.189	0.756	0.28		
19.3	^{124}Te	64.50	0.839	10.88	1.557	0.762				0.73	139	5.571
		125.92	0.729	9.88	1.552	0.786				0.72	261	5.355
		178.94	0.672	14.24	1.415	0.892				0.71	363	5.251
		181.56	0.634				18.85	0.835	1.165	0.65		
r_o = ..4 F r_c = 1.25 F												
19.95	^{123}Sb	77.9	0.658	7.62	1.701	0.464				1.20	243	5.920
		159.4	0.576	12.41	1.638	0.447				1.24	488	5.801
		241.3	0.538	16.08	1.623	0.393				1.24	733	5.750

Table 3 - Potential families obtained for α particles.

r_0 = 1.2 F	r_c = 1.25 F											
Energy (MeV)	Element	V_o (MeV)	a_o (F)	W_V (MeV)	r_V (F)	a_V (F)	W_S (MeV)	r_S (F)	a_S (F)	χ^2	J_o (MeV.F^3)	$\langle r_o^2\rangle^{1/2}$ (F)
19.5	^{123}Sb	83.48*	0.744	10.87	1.619	0.735				0.24	232	5.386
		134.47*	0.686	13.01	1.561	0.760				0.24	367	5.276
		196.24*	0.644	19.10	1.462	0.799				0.24	528	5.203
		233.47*	0.617	22.15	1.421	0.816				0.24	623	5.157
		84.51	0.747				17.21	1.260	0.809	0.25		
		134.11	0.688				25.11	1.182	0.816	0.25		
		194.85	0.630				26.02	1.108	0.881	0.25		
		232.94	0.626				39.57	1.065	0.842	0.25		
22.35	^{124}Sn	94.02	0.759	14.22	1.567	0.683				0.77	262	5.412
		184.12	0.673	21.64	1.476	0.706				0.76	499	5.253
		220.72	0.653	24.78	1.446	0.714				0.76	593	5.218
		180.77	0.480				41.75	1.172	0.715	0.77		
19.5	^{124}Te	66.45	0.734	7.53	1.716	0.762				0.67	183	5.364
		142.74	0.551	7.50	1.502	1.154				0.64	372	5.054
		205.15	0.557	12.48	1.340	1.174				0.64	536	5.063
		172.02	0.624				20.03	1.070	1.002	0.79		
19.5	^{122}Te	87.92	0.754	8.08	1.684	0.735				0.70	245	5.414
		136.39	0.695	8.29	1.668	0.760				0.69	372	5.304
		198.77	0.660	11.74	1.568	0.799				0.69	536	5.242
		235.30	0.644	13.39	1.530	0.816				0.66	631	5.214
		146.88	0.567				12.73	0.481	.689	0.38		

Table 4 - Potential families obtained for ^{3}He.

REACTION	E_{lab} (MeV)	V_o (MeV)	r_o (F)	a_o (F)	W_v (MeV)	r_v (F)	a_v (F)	χ^2
$^{124}Sn(^3He,^3He)^{124}Sn$	22.35	184.12	1.2	0.673	21.64	1.476	0.706	0.76
$^{124}Sn(\alpha,\alpha)^{124}Sn$	19.5	185.05	1.2	0.720	12.87	1.552	0.666	0.30
$^{123}Sb(^3He,^3He)^{123}Sb$	19.5	134.47	1.2	0.686	13.01	1.561	0.760	0.24
$^{123}Sb(\alpha,\alpha)^{123}Sb$	19.95	176.29	1.2	0.737	9.39	1.676	0.506	1.31
$^{124}Te(^3He,^3He)^{124}Te$	19.52	142.74	1.2	0.551	7.51	1.502	1.154	0.64
$^{124}Te(\alpha,\alpha)^{124}Te$	19.3	178.94	1.2	0.672	14.24	1.415	0.892	0.71
$^{122}Te(^3He,^3He)^{122}Te$	19.52	136.39	1.2	0.695	8.29	1.668	0.760	0.69

Table 5 - Best fit parameters.

REFERENCES

1. C.M. Perey and F.G. Perey, Nuclear Data Tables 10, 539 (1972).
2. R.L. Auble, J.B. Ball, Nucl. Phys. A179, 353 (1972).
3. P. Mailandt, J.S. Lilley and G.W. Greenlees, Phys. Rev. C8, 2189 (1973).
4. A. Szanto de Toledo, Master's thesis IFUSP (1970).
5. O. Sala and G. Spalek, Nucl. Instr. Meth. 122, 213 (1974).
6. V.H. Rotberg, Master's thesis IFUSP (1975).
7. D. Pereira, Master's thesis IFUSP (1975).
8. J.H. Hirata, Master's thesis IFUSP (1975).
9. H.R. Worthington, J.N. McGruer and D.E. Findley, Phys. Rev. 90, 899 (1953).
10. T. Polga, S.D. Paciornick and C.Z. Mammana, Proceedings of the " II Simpósio sobre o Treinamento de Físicos em Computação ", held in São Paulo.
11. J.M. Cohenca, *Computer Programme for Optical Model Analysis of Nuclear Scattering*, Nucl. Phys. Lab. Report n? 41, Univ. of Oxford (1968).
12. J.W. Luetzelschwab and J.C. Hafele, Phys. Rev. 180, 1023 (1969).
13. E.F. Gibson, B.W. Riedley, J.J. Kraushaar, M.E. Rickey and R. H. Bassel, Phys. Rev. 155, 1194 (1967).
14. P.P. Urone, L.W. Put, B.W. Ridley and G.D. Jones, Nucl. Phys. A167, 383 (1971).
15. D.J. Baugh, Nucl. Phys. A131, 417 (1969).
16. M.E. Cage, A.J. Cole and G.J. Pyle, Nucl. Phys. A201, 418 (1973).
17. J.S. Blair, Phys. Rev. 95, 1218 (1954).
18. D.C. Weisser, J.S. Lilley, R.K. Hobbie and G.W. Greenlees, Phys. Rev. C2, 544 (1970).
19. M.E. Cage, D.L. Clough, A.J. Cole, J.B.A. England, G.J. Pyle, P. M. Rolph, L.H. Watson and D.H. Worledge, Nucl. Phys. A183, 449 (1972).
20. G.W. Greenless, G.J. Pyle and Y.C. Tang, Phys. Rev. 171, 1115 (1968).
21. P.P. Urone, L.W. Put and B.W. Ridley, Nucl. Phys. A186, 344 (1972).
22. R. Bock, P. David, H.H. Duhm, H. Hefele, U. Lynen and R. Stock, Nucl. Phys. A92, 539 (1967).